

Article

Selecting the Degree of Partial Lithiation for Preventing Fracture in Si Micoparticles

Bo Wang ¹, Pu Hu ² and Katerina E. Aifantis ^{1,*}

¹ Department of Mechanical and Aerospace Engineering, University of Florida, Gainesville, FL 32608, USA; wangbo@ufl.edu

² Hubei Key Laboratory of Plasma Chemistry and Advanced Materials, Department of Materials Science and Engineering, Wuhan Institute of Technology, Wuhan 430205, China

* Correspondence: kafantis@ufl.edu

Abstract: The limiting aspect in commercializing Si-based anodes is the fractures they undergo during lithiation and de-lithiation. Experimental and theoretical studies have shown that this fracture is minimized when the particle size is reduced below 100 nm; however, this is not a commercially viable solution. Herein, we employ a multiphysics model to capture damage in 1 μm and 2 μm Si particles for different degrees of partial lithiation and corresponding de-lithiation. It is seen that partial lithiation can reduce the mechanical stresses experienced by the Si particles and fracture is fully prevented when the Li-ion penetration does not exceed 360 nm and 600 nm for 1 μm and 2 μm Si particles, respectively, when they are distributed in a binder containing smaller Si particles of 500 nm and 1 μm particles, respectively, prior to de-insertion. This indicates that limiting lithiation to 72% for 1 μm Si particles and 66% for 2 μm Si particles can prevent their pulverization. Removing the smaller Si particles and having a uniform Si size distribution results in lower lithiation states for preventing fracture. Such design information is vital for battery developers in order to fully utilize the capabilities of Si.

Keywords: multiphysics damage model; partial lithiation



Citation: Wang, B.; Hu, P.; Aifantis, K.E. Selecting the Degree of Partial Lithiation for Preventing Fracture in Si Micoparticles. *Batteries* **2023**, *9*, 324. <https://doi.org/10.3390/batteries9060324>

Academic Editors: Carolina Rosero-Navarro and Hirotoshi Yamada

Received: 5 April 2023

Revised: 29 May 2023

Accepted: 5 June 2023

Published: 13 June 2023



Copyright: © 2023 by the authors. Licensee MDPI, Basel, Switzerland. This article is an open access article distributed under the terms and conditions of the Creative Commons Attribution (CC BY) license (<https://creativecommons.org/licenses/by/4.0/>).

1. Introduction

Silicon-based anodes are the most promising Li-ion batteries due to their high theoretical capacities (over 3000 mAh/g compared to 372 mAh/g for graphite) and abundance in nature; however, they undergo colossal volume expansions of approximately 400% upon maximum lithiation [1–7]. This leads to severe damage and fracture, which reduces the active Si that can react with Li; therefore, the initial experimental capacity (>3000 mAh/g) [8] is significantly reduced during electrochemical cycling. Experimental [9,10] and theoretical [10,11] studies have shown that reducing the Si particle size below 100 nm can prevent damage of the individual particles in porous-type electrodes (Si + binder + additives). This fracture alleviation can interpret the very promising capacity retentions that have been achieved for nanoscale Si-based anodes, which range between 750 mAh/g for 1000 cycles [12], 1271 mAh/g for 1000 cycles [13], and 2312 mAh/g for 100 cycles [14]. In situ lithiation of individual Si particles has shown that fracture can be avoided for 380 nm Si particles (i.e., greater than 100 nm) [15]; however, the conditions in such cases are very different than those present in porous electrodes.

Mass producing nano-Si-based porous electrodes for the plethora applications of Li-ion batteries is prohibitive not only due to the cost of nanoparticles, but also the difficulty in preventing agglomeration during their fabrication and storage. Battery companies recently have begun commercializing Si-based anodes that contain very low Si contents with a particle size over 500 nm in order for the interparticle spacing to be large enough and have the binder act as a buffering agent to prevent fracture. Tuning the binder and interparticle spacing is a key factor in preventing fracture as earlier theoretical studies have shown [16];

however, another aspect that controls damage is the lithiation state. It was shown that full discharge of SiO particles at a C-rate of 1/24 led to the cracking of the particles with diameters greater than 2 μm near the surface, and pulverization of the particles with diameters greater than 10 μm [4]. Although partial lithiation of the silicon particles results in lower capacities (as the complete Si particle is not utilized), it corresponds to smaller volume changes (and hence damage) of the Si, which can result in electrochemical longevity, as numerous studies have shown [17–21]. Recently, it was illustrated that partial lithiation of Si microparticles in porous electrodes allowed for a significantly improved performance over 250 full cycles [22]. It was suggested that the improved performance was related to the reduction in mechanical stresses with partial lithiation; however, a more recent study indicated that partial lithiation also allowed the retention of Si crystallinity, which can also improve cyclability [23].

In order to fully understand how to utilize partial lithiation, it is necessary to probe its relationship to Si damage and fracture during cycling. From an electrochemical point of view, it was shown experimentally that for 4.5 μm Si-particle porous electrodes, the partial lithiation should not exceed 30% in order to attain a stable capacity for 250 full cycles [22]. It was assumed that damage increased at higher lithiation states resulting in the observed capacity decay; however, only a single scanning electron microscopy image was provided showing a very small area of Si to support this hypothesis. Herein, we therefore perform a numerical analysis in order to document the development of damage for different partial lithiation states for microscale Si particles embedded in a polymer. In order to study the effect of particle size and particle distribution (within the porous electrode) on fracture, four cases are considered: that of small and larger Si particles distributed within a polymer binder (the large Si particles are either 1 or 2 μm), and the case of only same size larger Si particles embedded in the binder (again with diameters of either 1 or 2 μm). This is the first study that provides a correlation between partial lithiation and damage that can aid battery developers in employing micron Si particles, without having to keep their volume fractions low. In addition to Si particles, this numerical model can be applied to other types of active particles (such as germanium or tin) that can be used in Li-ion and Na-ion batteries.

2. Modeling

In order to reduce computation time, a 2D (rather than 3D) representation will be employed. In this study, several square polymer binders embedded with multiple Si particles are considered. There are two different configurations. In the first case, there are five bigger Si particles and four smaller Si particles embedded in the polymer binder, in which the radii of the smaller particles are only one half of the larger ones. In the second case, the smaller particles are removed and only the larger ones are considered. To start with, a square polymer binder of 6400 nm \times 6400 nm with both small and large particles is considered, with diameters of 500 nm and 1 μm , respectively. The spacing between two adjacent 1 μm particles (in either the horizontal or vertical directions) is 1600 nm. To evaluate the damage evolution of this 2D configuration during lithiation, a phase field damage model coupled with the diffusion equation with a nonlinear concentration-dependent diffusivity is adopted [10,24,25]. This model has been experimentally verified as it was successfully applied to capture the dry lake-bed fracture pattern in Si thin-film electrodes [24], the critical particle size of Si below which no fracture would occur during full lithiation [10], and the composition of cathodes that would alleviate damage during sodiation [25].

Lithium transport can be expressed by Fick's law as [10,24,25]:

$$\frac{\partial c^*}{\partial t} = D \nabla^2 c^* \quad (1)$$

where the concentration-dependent diffusivity parameter D is given by $D = D_0 \left(\frac{1}{1-c^*} - 2 \times 1.95 \times c^* \right)$ and c^* denotes the normalized/relative Li-ion concentration, equal to the actual molar concentration of Li-ions per unit volume divided by the maximum

Li-ion concentration. c^* is dimensionless and can range from 0 to 1, corresponding to the fully de-lithiated state (pure Si) and completely lithiated state ($\text{Li}_{3.75}\text{Si}$ at room temperature), respectively. D_0 is the initial diffusivity, when no Li-ions are present in the Si, i.e., $c^* = 0$. As for the mechanical part, small deformation theory is adopted. The total strain $\boldsymbol{\varepsilon}_t$ can be decomposed as the sum of the stress-free strain $\boldsymbol{\varepsilon}_c$ which is induced by Li-ion diffusion and the elastic strain $\boldsymbol{\varepsilon}_e$:

$$\boldsymbol{\varepsilon}_t = \frac{1}{2} \left\{ (\nabla \mathbf{u}) + (\nabla \mathbf{u})^T \right\} = \boldsymbol{\varepsilon}_e + \boldsymbol{\varepsilon}_c \quad (2)$$

where

$$\boldsymbol{\varepsilon}_c = \alpha c^* \mathbf{I} \quad (3)$$

\mathbf{I} is the second-order unit tensor, \mathbf{u} is the displacement field, α is the dilatation coefficient (analogy to thermal expansion coefficient) and a negative α is needed for de-lithiation. The equilibrium equation (balance of linear momentum) is given by:

$$\nabla \cdot \boldsymbol{\sigma} = 0 \quad (4)$$

where $\boldsymbol{\sigma}$ is the Cauchy stress tensor. Furthermore, the governing equation for the damage filed can be described by [26]:

$$-l^2 \Delta d + d = \frac{2l}{G_c} (1 - d) \quad (5)$$

where the phase field variable d can only grow from 0 to 1 (corresponding to the intact state and fully broken state, respectively), G_c is material-dependent Griffith's critical energy release rate (the energy required to create a fracture surface per unit area), and l is an internal length scale characteristic of the material. \mathcal{H} is a history variable that is the maximum elastic strain energy density over time. The initial conditions are concentration $c^* = 0$ and damage $d = 0$ for lithiation. Similar to the dilatation coefficient, a negative ion flux is adopted for de-lithiation. In addition, the initial conditions for the concentration and damage field come from the results after full lithiation. The boundary conditions for this Li/electrode system are a constant flux of Li-ions (1.4 nm/ms [24]) at the exterior surface of the electrode and the symmetry displacement boundary conditions for the outer surfaces of the polymer [27]. The Young's modulus of the Si particles is 130 GPa, while the polymer is taken to be composed of the common binder.

α is set as 0.3 [24] for the Si electrode, while for the binder it is assumed to be zero, since it is taken to be inert with respect to Li and therefore cannot host Li-ions. The energy release rate for the Si electrodes was determined to be 10–12 J/m² [28]. It should be noted that if the experimental value is adopted for G_c , a much lower internal length is needed to obtain the desired fracture patterns. Thus, a more refined mesh is needed which is relatively computationally expensive. In the present study, G_c for the Si particles is 50 J/m². The internal length is a material constant that depends on the microstructure and cannot be larger than the particle; hence, for the Si it is taken to be 50 nm. For an ideal Si-based electrode, the polymer surrounding the Si would not fracture, and in order for the model to capture this, the energy release rate for the polymer is taken to be 100 times higher than that of Si.

The governing equations are solved in the open-source software FEniCS by employing an unstructured mesh that has a size approximately 1/100 of the side length of the polymer. The Euler backward method is employed for the discretization of the diffusion equations and the time step size is chosen as 400 sec. It takes 110 steps (approximately 12 h) to complete a full lithiation or another 110 steps for complete de-lithiation. The full lithiation refers to the state of the battery in which the anode material of the battery exhibits its highest loading of lithium.

3. Results and Discussion

To investigate the relationship between partial lithiation and Si fracture, the damage evolution for different lithiation states was obtained. The concentration profiles provide the distance within the Si particle over which the Li-ions diffuse and therefore the percentage of Li within the Si was estimated for various partial lithiation states. To eliminate unrealistic damage, after lithiation and before de-lithiation, the value of damage is initialized to 0 except when it was higher than 0.9. This allows the electrode to store elastic energy again, avoiding the effect of damage values close to 0.5 that are somehow unrealistic. Damage profiles after full and partial lithiation and de-lithiation are shown in Figure 1. It should be noted that for the case of partial lithiation, once the specified partial lithiation was reached, de-lithiation took place.

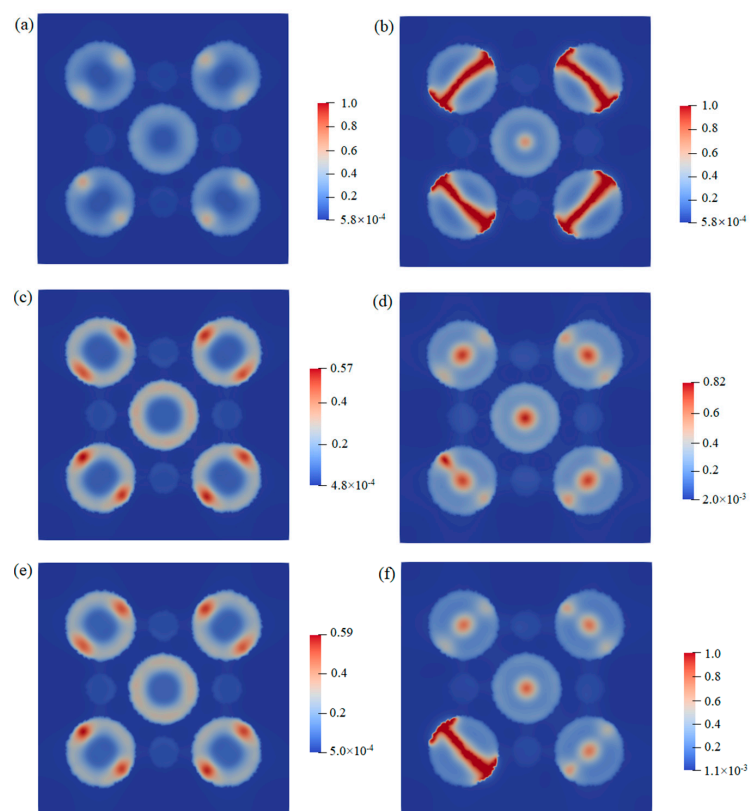


Figure 1. Damage profiles of Si particles embedded in PVDF; radii of larger and smaller particles are 500 nm and 250 nm, respectively, (a,b) for lithiation and de-lithiation. (c,d) A total of 67% lithiation and respective de-lithiation. (e,f) A total of 72% lithiation and respective de-lithiation.

To investigate the relationship between partial lithiation and Si fracture, the damage evolution for different lithiation states was obtained. The concentration profiles provide the distance within the Si particle over which the Li-ions diffuse and therefore the percentage of Li within the Si was estimated for various partial lithiation states. To eliminate unrealistic damage, after lithiation and before de-lithiation, the value of damage was initialized to 0 except for when it was higher than 0.9. This allows the electrode to store elastic energy again, avoiding the effect of damage values close to 0.5 that are somehow unrealistic. Damage profiles after full and partial lithiation and de-lithiation are shown in Figure 1. It should be noted that for the case of partial lithiation, once the specified partial lithiation was reached, de-lithiation took place.

Based on the simulation results, it is seen that cracks begin to initiate in the 1 μm particles after complete lithiation (110 time steps, i.e., 12.2 h) and continue to propagate during the de-lithiation process cutting the particles in half. This has been shown to be in agreement with experiments, as 1 μm Si particles in porous electrodes fractured in

this manner upon complete lithiation [10]. If the lithiation degree of the particle is 67% (104 time steps, i.e., 11.56 h), the damage after one cycle is less than 0.9, and can therefore be neglected. However, once the partial lithiation degree is greater than 72% (105 time steps, i.e., 11.67 h), it will lead to fracture in the 1 μm Si particles. In particular, it is seen that even if the damage is negligible, after 72% lithiation of the Si, once de-lithiation takes place at this partial lithiation state, fracture begins to occur in some particles.

To study the influence of particle size on the fracture pattern, the same configuration as shown in Figure 1 is used but the sizes for both the polymer and particles are doubled, i.e., the size of the polymer binder is 12,800 nm \times 12,800 nm and the radii of the smaller and larger particles are 1 μm and 2 μm , respectively. The ion flux is 1.2 nm/ms and the time step size is chosen as 800 s. The other parameters are the same as before. It takes 250 steps (approximately 55.6 h) to complete a full lithiation and another 250 steps for complete de-lithiation. Damage profiles after full and partial lithiation and de-lithiation are shown in Figure 2. The damage profile (Figure 2b) after full lithiation is also similar to the previous case (Figure 1b) with smaller particle sizes since, again, there are four Si particles cut into halves. When the particle size is increased, however, more decohesion (i.e., detachment of the active material from the binder) takes place, as seen in Figure 2. The damage profiles after partial lithiation and de-lithiation are also similar between the cases in Figures 1 and 2; however, a different critical partial lithiation state to prevent fracture is noted. Figure 2c–f show the damage profiles after 60% (212 time steps, i.e., 47.1 h) and 64% (213 time steps, i.e., 47.3 h) lithiation and de-lithiation, respectively. In particular, it is found that the critical lithiation degree for the configuration in Figure 2 is 64%.

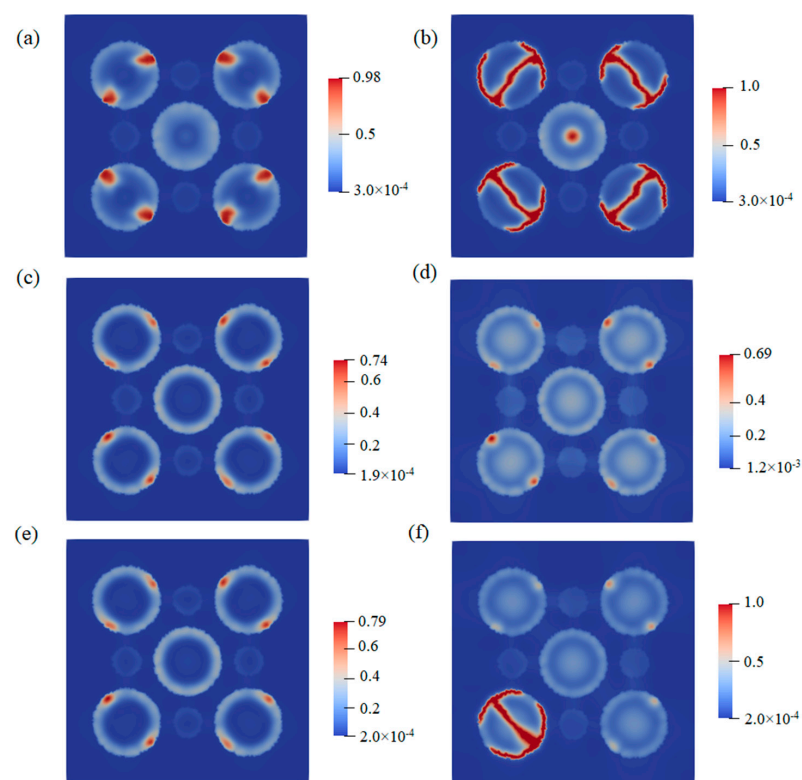


Figure 2. Damage profiles of Si particles with radii of 1 μm and 500 nm, respectively. (a,b) Full lithiation and de-lithiation. (c,d) A total of 60% lithiation and de-lithiation. (e,f) A total of 64% lithiation and de-lithiation.

As mentioned, the lithiation states were estimated from the concentration profiles. This is illustrated in Figure 3, which corresponds to the critical partial lithiation case where fracture began to take place upon de-lithiation. It is seen that when the radius of the large Si particles was 500 nm, fracture was fully prevented in the square domain of

$6400 \text{ nm} \times 6400 \text{ nm}$ when the Li-ion penetration did not exceed 360 nm , which corresponds to 72% lithiation of the particle (as shown in Figure 3a). This means that limiting the lithiation state below this critical value can prevent fracture and crack growth in $1 \mu\text{m}$ Si particles, enhancing the electrochemical performance. It should be noted that the small Si particles of 500 nm did not experience damage for this lithiation state, illustrating that the lithiation state affecting damage is size dependent and must be considered separately for each particle size.

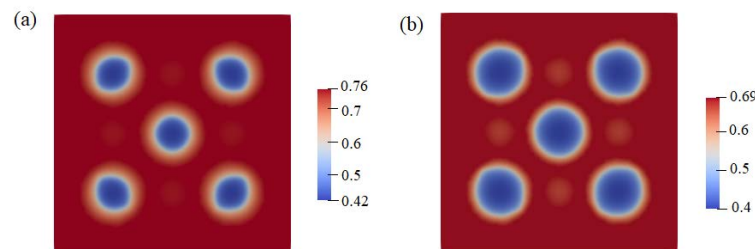


Figure 3. Concentration profile of Si particles with (a) radii of 500 nm and 250 nm with 72% lithiation of the particle, and (b) radii of $1 \mu\text{m}$ and 500 nm with 64% lithiation of the particle.

To have a better understanding of the configurations on the fracture pattern, more simulations were performed. Compared to the previous simulations (Figures 1 and 2), the smaller particles are removed and only the larger ones are considered. All the other parameters are kept the same as in the previous cases. For the Si particles with 500 nm radii and square domain of $6400 \text{ nm} \times 6400 \text{ nm}$, the damage profiles are shown in Figure 4. It takes 12 h to complete the full lithiation. The damage profiles after full lithiation and de-lithiation are shown in Figure 4a,b, while Figure 4c–f show those after 62% lithiation for 10 h and 66% lithiation for 10.2 h lithiation and de-lithiation, respectively.

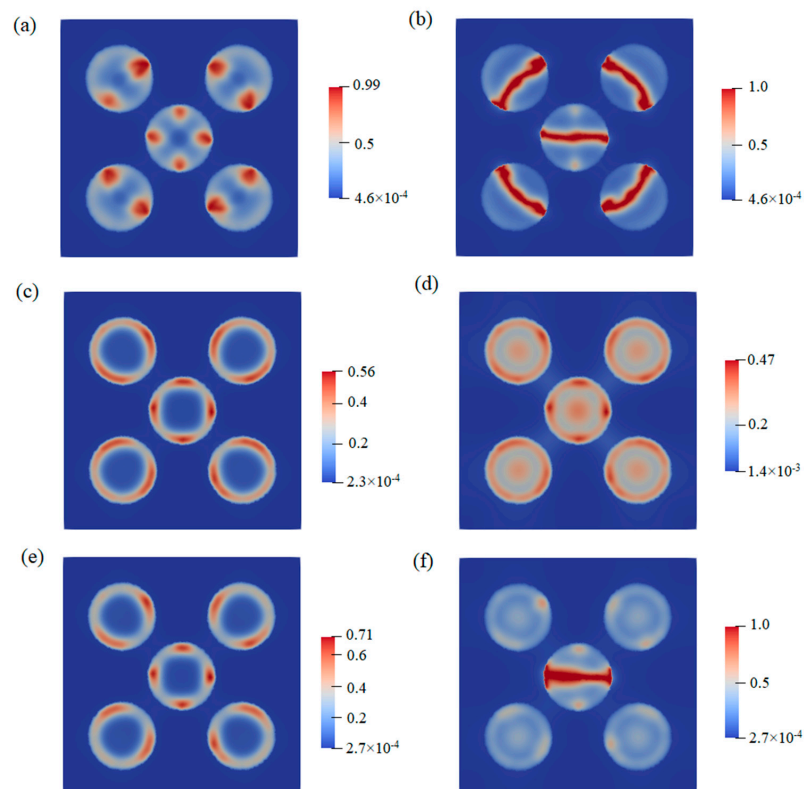


Figure 4. Damage profiles of Si particles with a radius of 500 nm after lithiation (a,c,e) and de-lithiation (b,d,f). (a,b) Full lithiation and de-lithiation. (c,d) A total of 62% lithiation and de-lithiation. (e,f) A total of 66% lithiation and de-lithiation.

In particular, it is found that the critical lithiation degree to prevent fracture for this configuration is 66%. Similarly, for the Si particles with a radius of 1 micron and square domain of $12,800 \text{ nm} \times 12,800 \text{ nm}$, the damage profiles are depicted in Figure 5. It takes 54 h to complete the full lithiation. The damage profiles after full lithiation and de-lithiation are shown in Figure 5a,b, while Figure 5c–f show the damage profiles after 58% lithiation for 45.4 h and 60% lithiation for 45.6 h, respectively. In particular, it is found that the critical lithiation degree preventing fracture of the Si for this case is 60%. The concentration profiles for the critical lithiation states for Figures 4 and 5 are plotted in Figure 6, providing a maximum Li-ion concentration and the penetration depths of 320 mm and 580 mm to prevent fracture in geometries containing only large 1 micron and 2 micron Si particles, respectively.

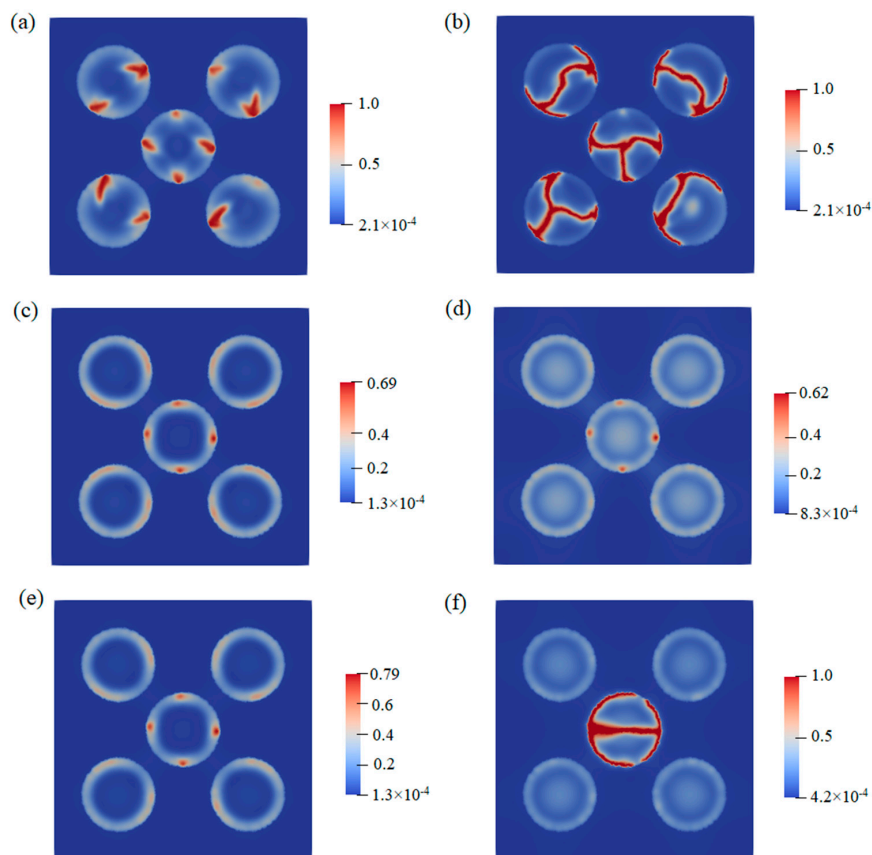


Figure 5. Damage profiles of Si particles with a radius of $1 \mu\text{m}$ after lithiation (a,c,e) and de-lithiation (b,d,f). (a,b) Full lithiation and de-lithiation. (c,d) A total of 58% lithiation and de-lithiation. (e,f) A total of 60% lithiation and de-lithiation.

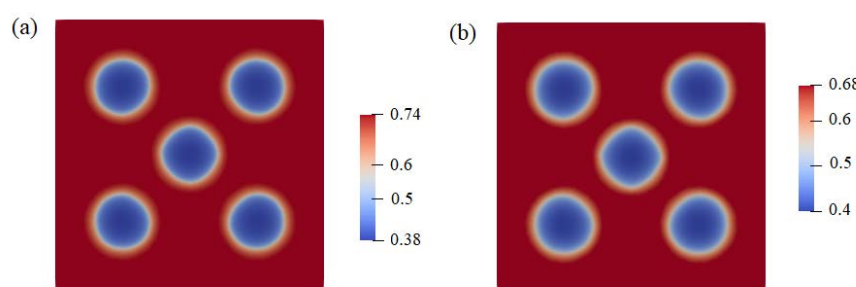


Figure 6. Concentration profile of Si particles with (a) radii of 500 nm with 66% lithiation of the particle, and (b) radii of $1 \mu\text{m}$ with 60% lithiation of the particle.

By taking a closer look at these damage profiles, it can be concluded that the fracture pattern depends on the particle size, lithiation state, and the configuration of the Si binder system. An interesting finding is that when there are less particles present, cracks begin to initiate and propagate within the center of the particle. This is due to the fact that Li-ion diffusion is more difficult when the central particle is surrounded by smaller particles. As a result, the concentration gradient is less severe, leading to relatively less damages in the configurations containing a distribution of small and large Si particles. The present results are not complemented by respective experiments, as documenting morphology changes during partial lithiation is time consuming and tedious. However, the proposed design configurations are currently being considered experimentally and the results will be reported in the future.

4. Conclusions

Partial lithiation of Si microparticles has been proposed as a promising avenue for reducing the mechanical stresses experienced during lithiation and increasing their electrochemical stability. Herein, we employed a multiphysics phase field model for capturing the damage for various degrees of partial lithiation in 1 μm and 2 μm Si particles embedded in a polymer binder. Cases where secondary (smaller) Si particles were also dispersed in the binder were considered. In doing so, we were able to illustrate that in order to prevent fracture for the case where both 1 μm Si particles and 500 nm Si particles were embedded in PVDF, the lithium penetration depth should not exceed 360 nm in the 1 micron particles. This indicates that in order to successfully utilize 1 μm Si particles that do not degrade during cycling, their degree of partial lithiation should not exceed 72%. For the case where a larger set of particles was embedded in the binder (2 μm and 1 μm Si particles), the lithium penetration depth should not exceed 600 nm (corresponding to a 64% lithiation degree) in order to prevent fracture during electrochemical cycling. If there are no smaller particles present, the critical lithiation degree for preventing fracture is 66% and 60%, respectively, for 1 μm and 2 μm Si particles. This illustrates that the partial lithiation degree value is size dependent and will also be affected by the binder which constrains the Si volume expansions. For each binder type and particle size system, there is a different maximum partial lithiation state that will allow for the most promising mechanical stability and, hence, prolonged cyclability. This methodology can also aid in the design of other types of Li- and Na-based battery systems that employ active particles dispersed within a binder or even solid electrolyte.

Author Contributions: Conceptualization, B.W. and K.E.A.; methodology, B.W. and K.E.A.; software, B.W.; validation, P.H. and K.E.A.; formal analysis, B.W., K.E.A. and P.H.; investigation, B.W. and K.E.A.; resources, K.E.A.; data curation, B.W., K.E.A. and P.H.; writing—original draft preparation, B.W. and K.E.A.; writing—review and editing, B.W. and K.E.A.; visualization, B.W., K.E.A. and P.H.; supervision, K.E.A.; project administration, K.E.A.; funding acquisition, K.E.A. All authors have read and agreed to the published version of the manuscript.

Funding: This research was funded by the U.S. National Science Foundation grant number CMMI-1762602.

Institutional Review Board Statement: Not applicable.

Informed Consent Statement: Not applicable.

Data Availability Statement: The data presented in this study are available upon request from the corresponding author.

Acknowledgments: The authors are grateful to the U.S. National Science Foundation for supporting this work through the CMMI grant (CMMI-1762602).

Conflicts of Interest: The authors declare no conflict of interest.

References

- Beaulieu, L.; Eberman, K.; Turner, R.; Krause, L.; Dahn, J. Failure modes of silicon powder negative electrode for lithium secondary batteries. *Electrochim. Solid State Lett.* **2001**, *4*, A137. [[CrossRef](#)]
- Obrovac, M.; Christensen, L.; Le, D.B.; Dahn, J.R. Alloy design for lithium-ion battery anodes. *J. Electrochem. Soc.* **2007**, *154*, A849. [[CrossRef](#)]
- Laokawee, V.; Jarulertwattana, N.; Susingrat, W.; Sarakonsri, T. Synthesis of silicon-tin/nitrogen-doped reduced graphene oxide nanocomposite as anode materials for lithium-ion batteries. *Mater. Today Proc.* **2019**, *17*, 1302–1308. [[CrossRef](#)]
- Hovington, P.; Dontigny, M.; Guerfi, A.; Trottier, J.; Lagacé, M.; Mauger, A.; Julien, C.; Zaghib, K. In situ Scanning electron microscope study and microstructural evolution of nano silicon anode for high energy Li-ion batteries. *J. Power Source* **2014**, *248*, 457–464. [[CrossRef](#)]
- Zhang, L.; Al-Mamun, M.; Wang, L.; Dou, Y.; Qu, L.; Dou, S.X.; Liu, H.K.; Zhao, H. The typical structural evolution of silicon anode. *Cell Rep. Phys. Sci.* **2022**, *3*, 100811. [[CrossRef](#)]
- Leblanc, D.; Guerfi, A.; Cho, M.; Paoletta, A.; Wang, Y.; Mauger, A.; Julien, C.; Zaghib, K. Advanced silicon-based electrodes for high-energy lithium-ion batteries. In *Silicon Anode Systems for Lithium-Ion Batteries*; Elsevier: Amsterdam, The Netherlands, 2022; pp. 411–456.
- Sun, L.; Liu, Y.; Shao, R.; Wu, J.; Jiang, R.; Jin, Z. Recent progress and future perspective on practical silicon anode-based lithium ion batteries. *Energy Storage Mater.* **2022**, *46*, 482–502. [[CrossRef](#)]
- Li, H.; Huang, X.; Chen, L.; Wu, Z.; Liang, Y. A high capacity nano Si composite anode material for lithium rechargeable batteries. *Electrochim. Solid-State Lett.* **1999**, *2*, 547–549. [[CrossRef](#)]
- Liu, X.H.; Zhong, L.; Huang, S.; Mao, S.X.; Zhu, T.; Huang, J.Y. Size-dependent fracture of silicon nanoparticles during lithiation. *ACS Nano* **2012**, *6*, 1522–1531. [[CrossRef](#)]
- Ahuja, U.; Wang, B.; Hu, P.; Rethore, J.; Aifantis, K.E. Polydopamine coated Si nanoparticles allow for improved mechanical and electrochemical stability. *Electrochim. Acta* **2021**, *392*, 138993. [[CrossRef](#)]
- Luo, F.; Liu, B.; Zheng, J.; Chu, G.; Zhong, K.; Li, H.; Huang, X.; Chen, L. Nano-silicon/carbon composite anode materials towards practical application for next generation Li-ion batteries. *J. Electrochem. Soc.* **2015**, *162*, A2509. [[CrossRef](#)]
- Li, X.; Gu, M.; Hu, S.; Kennard, R.; Yan, P.; Chen, X.; Wang, C.; Sailor, M.J.; Zhang, J.G.; Liu, J. Mesoporous silicon sponge as an anti-pulverization structure for high-performance lithium-ion battery anodes. *Nat. Commun.* **2014**, *5*, 4105. [[CrossRef](#)]
- An, W.; Gao, B.; Mei, S.; Xiang, B.; Fu, J.; Wang, L.; Zhang, Q.; Chu, P.K.; Huo, K. Scalable synthesis of ant-nest-like bulk porous silicon for high-performance lithium-ion battery anodes. *Nat. Commun.* **2019**, *10*, 1447. [[CrossRef](#)]
- Malik, Y.T.; Shin, S.Y.; Jang, J.I.; Kim, H.M.; Cho, S.; Do, Y.R.; Jeon, J.W. Self-Repairable Silicon Anodes Using a Multifunctional Binder for High-Performance Lithium-Ion Batteries. *Small* **2023**, *19*, 2206141. [[CrossRef](#)] [[PubMed](#)]
- Wang, C.M.; Luo, L. In-situ TEM Study of Coating Layer Function on Silicon Anode Particle for Lithium Ion Battery. *Microsc. Microanal.* **2016**, *22*, 1324–1325. [[CrossRef](#)]
- Dimitrijevic, B.; Aifantis, K.; Hackl, K. The influence of particle size and spacing on the fragmentation of nanocomposite anodes for Li batteries. *J. Power Sources* **2012**, *206*, 343–348. [[CrossRef](#)]
- Dimov, N.; Fukuda, K.; Umeno, T.; Kugino, S.; Yoshio, M. Characterization of carbon-coated silicon: Structural evolution and possible limitations. *J. Power Sources* **2003**, *114*, 88–95. [[CrossRef](#)]
- Kierzek, K.; Machnikowski, J. Factors influencing cycle-life of full Li-ion cell built from Si/C composite as anode and conventional cathodic material. *Electrochim. Acta* **2016**, *192*, 475–481. [[CrossRef](#)]
- Laik, B.; Ung, D.; Caillard, A.; Sorin Cojocaru, C.; Pribat, D.; Pereira-Ramos, J.P. An electrochemical and structural investigation of silicon nanowires as negative electrode for Li-ion batteries. *J. Solid State Electrochem.* **2010**, *14*, 1835–1839. [[CrossRef](#)]
- Li, Y.; Lu, B.; Guo, B.; Song, Y.; Zhang, J. Partial lithiation strategies for suppressing degradation of silicon composite electrodes. *Electrochim. Acta* **2019**, *295*, 778–786. [[CrossRef](#)]
- Haufe, S.; Ranninger, J.; Bernhard, R.; Buchberger, I.; Hanelt, E. Improving Cycle Life of Silicon-Dominant Anodes Based on Microscale Silicon Particles under Partial Lithiation. *Batteries* **2023**, *9*, 58. [[CrossRef](#)]
- Jantke, D.; Bernhard, R.; Hanelt, E.; Buhrmester, T.; Pfeiffer, J.; Haufe, S. Silicon-dominant anodes based on microscale silicon particles under partial lithiation with high capacity and cycle stability. *J. Electrochem. Soc.* **2019**, *166*, A3881. [[CrossRef](#)]
- Graf, M.; Berg, C.; Bernhard, R.; Haufe, S.; Pfeiffer, J.; Gasteiger, H.A. Effect and Progress of the Amorphization Process for Microscale Silicon Particles under Partial Lithiation as Active Material in Lithium-Ion Batteries. *J. Electrochem. Soc.* **2022**, *169*, 020536. [[CrossRef](#)]
- Réthoré, J.; Zheng, H.; Li, H.; Li, J.; Aifantis, K.E. A multiphysics model that can capture crack patterns in Si thin films based on their microstructure. *J. Power Sources* **2018**, *400*, 383–391. [[CrossRef](#)]
- Hu, P.; Peng, W.; Wang, B.; Xiao, D.; Ahuja, U.; Réthoré, J.; Aifantis, K.E. Concentration-gradient Prussian blue cathodes for Na-ion batteries. *ACS Energy Lett.* **2019**, *5*, 100–108. [[CrossRef](#)]
- Nguyen, T.T.; Yvonnet, J.; Zhu, Q.Z.; Bornert, M.; Chateau, C. A phase field method to simulate crack nucleation and propagation in strongly heterogeneous materials from direct imaging of their microstructure. *Eng. Fract. Mech.* **2015**, *139*, 18–39. [[CrossRef](#)]

27. Rahani, E.K.; Shenoy, V.B. Role of plastic deformation of binder on stress evolution during charging and discharging in lithium-ion battery negative electrodes. *J. Electrochem. Soc.* **2013**, *160*, A1153. [[CrossRef](#)]
28. Choi, Y.S.; Pharr, M.; Oh, K.H.; Vlassak, J.J. A simple technique for measuring the fracture energy of lithiated thin-film silicon electrodes at various lithium concentrations. *J. Power Source* **2015**, *294*, 159–166. [[CrossRef](#)]

Disclaimer/Publisher’s Note: The statements, opinions and data contained in all publications are solely those of the individual author(s) and contributor(s) and not of MDPI and/or the editor(s). MDPI and/or the editor(s) disclaim responsibility for any injury to people or property resulting from any ideas, methods, instructions or products referred to in the content.